(γ, 2e) photo-double ionization of N_2 molecules for equal energy sharing

2013 J. Phys. B: At. Mol. Opt. Phys. 46 185203

(http://iopscience.iop.org/0953-4075/46/18/185203)

J. Phys. B: At. Mol. Opt. Phys. **46** (2013) 185203 (9pp) doi:10.1088/0953-4075/46/18/185203

$(\gamma, 2e)$ photo-double ionization of N_2 molecules for equal energy sharing

A A Bulychev[1], O Chuluunbaatar[1,2], A A Gusev[1] and B Joulakian[3]

[1] Joint Institute for Nuclear Research, Dubna, Moscow Region 141980, Russia
[2] National University of Mongolia, Ulaanbaatar, Mongolia
[3] Université de Lorraine, SRSMC (UMR CNRS 7565), 1 bld Arago, bat. ICPM F-57078, Metz Cedex 3, France

E-mail: boghos.joulakian@univ-lorraine.fr

Received 22 April 2013, in final form 19 August 2013
Published 6 September 2013
Online at stacks.iop.org/JPhysB/46/185203

Abstract
We have determined the multiply differential cross sections (MDCS) of the vertical photo-double ionization of diatomic nitrogen with coincidence detection of the ejected electrons, for fixed and random orientations of the internuclear axis, using the correlated product of two two-centre continuum Coulomb functions for the description of the two ejected electrons, which satisfies the exact asymptotic conditions. To verify our procedure, we have applied it to the photo-double ionization of diatomic hydrogen for which many experimental and theoretical results are available. Our results on diatomic hydrogen show the influence of the initial state correlation. In the case of diatomic nitrogen only, the photo-double ionization of the $3\sigma_g$ orbital is considered resulting in the $^1\Sigma_g$ state of the residual N_2^{2+} dication. The case of the nearby $^3\Pi_u$ final state having an open shell configuration will be considered in a future paper. Our results confirm the symmetry properties of the MDCS and give the optimal ejection angles. A comparison is also made with results obtained by the Gaussian parametrization method.

(Some figures may appear in colour only in the online journal)

1. Introduction

The double ionization by a single polarized photon is one of the principle experimental means to study the electronic structure of atoms and molecules and to probe electron–electron correlation, which is the main factor which causes double ionization of a target [1–3]. An abundant literature is available for the particular case of $(\gamma, 2e)$ photo-double ionization, where the two ejected electrons are detected in coincidence, especially for the helium and rare gas targets. See [4–9] for the experimental aspects of this process, and [10–17] for some of the theoretical approaches. In the case of diatomic targets, theoretical results are relatively less frequent for the multiply differential cross section (MDCS) [18], in spite of the fact that experimental detection of the ejected electrons from stable, naturally existing diatomic targets like H_2 or N_2 is quite similar to that of atoms like helium or nitrogen. This may come from the lack of theoretical support. In fact, after eliminating the rotational and vibrational movements of the diatomic target (for that see [19]), describing conveniently the two ejected electrons in the field of two attractive centres remains much more difficult than in the atomic case [20–24].

To our knowledge, in spite of the large interest on molecular dications in astrophysics and plasma science, dications being very abundant in the ionosphere of many planets and in interstellar clouds, no MDCS values are available for the $(\gamma, 2e)$ photo-double ionization of diatomic nitrogen with coincidence detection of the two ejected electrons and the residual $N^+(^3P)$ ion. In fact the potential energy of the fundamental state of N_2^{2+} has a potential well around the equilibrium internuclear distance whose minimum is higher than the level of the $N^+(^3P)$–$N^+(^3P)$ separated ions [25, 26]. This can be exploited in $(\gamma, 2e)$ dissociative ionization experiments with coincidence detection of the residual N^+ fragments with the two ejected electrons. This type of coincidence detection can give the orientation of the initial target and permit the observation of two-centre interference phenomena [27–29]. Similar complete experiments have been performed recently in the case of dissociative $(e, 2e)$ simple

ionization of diatomic hydrogen by electrons [30], where the emerging proton was detected in coincidence with the ejected electron.

The aim of the present work is to give the first MDCS of $(\gamma, 2e)$ photo-double ionization of the $3\sigma_g$ orbital of N_2 resulting in the $^1\Sigma_g$ state of the residual N_2^{2+} dication. The case of the ionization to the neighbouring $^3\Pi_u$ final state of N_2^{2+} [31, 32], which has an open shell electronic configuration, will be treated in a future paper. We extend here the computational procedure with which we have recently obtained [33] the MDCS of the $(e, 3e)$ double ionization of N_2 and H_2 in which we have applied the two-centre double continuum function [29]. This has given a better agreement with the experimental results on the $(e, 3e-1)$ double ionization of the hydrogen molecule [34], and has shown that the introduction of the electron–electron correlation in the final state is necessary.

2. Theory

Following Chang and Fano [35] and Ijima *et al* [19], we admit that the target, during the inelastic collision, is found in its fundamental electronic vibrational and rotational state and apply the closure relation on all of the vibrational and rotational levels of the final $^1\Sigma_g$ state of the residual N_2^{2+} dication [19]. The MDCS of the photo-double ionization for fixed internuclear distance $\boldsymbol{\rho}$ and orientation can then be written in atomic units by

$$\sigma^{(4)}(\boldsymbol{\rho}) = \frac{\mathrm{d}^4\sigma}{\mathrm{d}\Omega_\rho \mathrm{d}\Omega_1 \mathrm{d}\Omega_2\, \mathrm{d}(k_1^2/2)} = \frac{4\pi^2}{\omega}\alpha k_1 k_2 |T_{fi}|^2, \quad (1)$$

where $\mathrm{d}\Omega_1$, $\mathrm{d}\Omega_2$ and $\mathrm{d}\Omega_\rho$ are respectively the elements of the solid angles for the orientations of the ejected electrons and the internuclear axis. k_1 and k_2 represent the moduli of the wave vectors of the ejected electrons. $\alpha = 7.297\,35 \times 10^{-3}$ is the fine-structure constant, ω is the photon frequency. In the case of randomly oriented targets, we must pass to the triple differential cross section (TDCS) by integrating over all possible and equally probable directions of the molecule in space

$$\sigma^{(3)} = \frac{1}{4\pi}\int \mathrm{d}\Omega_\rho \sigma^{(4)}(\boldsymbol{\rho}). \quad (2)$$

The conservation of the energy, for fixed internuclear distance ρ, gives

$$E_f = E_1 + E_2 = E_i + \omega, \quad (3)$$

where $E_1 = k_1^2/2, E_2 = k_2^2/2$ represent respectively the energy values of the ejected electrons. E_i represents the energy needed to free the two bound electrons in N_2. We define the transition matrix element

$$T_{fi} = \int \mathbf{dr}_1 \int \mathbf{dr}_2 \bar{\chi}_f(\mathbf{r}_1, \mathbf{r}_2) V \varphi_i(\mathbf{r}_1, \mathbf{r}_2). \quad (4)$$

Here V is given in the velocity gauge by

$$V = \boldsymbol{\epsilon}\,(\boldsymbol{\nabla}_{r_1} + \boldsymbol{\nabla}_{r_2}) \quad (5)$$

with $\boldsymbol{\epsilon}$ representing the polarization vector for the photon. In the length gauge, it can be given by

$$V = -\omega\boldsymbol{\epsilon}\,(\mathbf{r}_1 + \mathbf{r}_2). \quad (6)$$

The symmetrized final state wave function describing the state of the two equivalent ejected electrons coming from the same molecular orbit is written in the following form

$$\chi_f(\mathbf{r}_1, \mathbf{r}_2) = \frac{\phi_f(\mathbf{k}_1, \mathbf{r}_1, \mathbf{k}_2, \mathbf{r}_2) + \phi_f(\mathbf{k}_1, \mathbf{r}_2, \mathbf{k}_2, \mathbf{r}_1)}{\sqrt{2}}. \quad (7)$$

Here

$$\phi_f(\mathbf{k}_1, \mathbf{r}_1, \mathbf{k}_2, \mathbf{r}_2) = v(k_{12})\,{}_1F_1 \times (\imath\alpha_{12}, 1, -\imath(k_{12}r_{12} + \mathbf{k}_{12}\mathbf{r}_{12}))T(\mathbf{k}_1, \mathbf{r}_1)T(\mathbf{k}_2, \mathbf{r}_2), \quad (8)$$

in which we have introduced, like in the case of atoms [36], the electron–electron correlation. $\mathbf{r}_{12} = \mathbf{r}_1 - \mathbf{r}_2$ gives the relative position of the two electrons, and

$$v(k_{12}) = \exp\left(-\frac{\pi\alpha_{12}}{2}\right)\Gamma\,(1 - \imath\alpha_{12})\,, \quad (9)$$

represents the Gamow factor with

$$\alpha_{12} = \frac{1}{2k_{12}}, \qquad \mathbf{k}_{12} = \frac{1}{2}(\mathbf{k}_1 - \mathbf{k}_2). \quad (10)$$

The final state wave function satisfies the ortho-normality condition in the sense

$$\langle\phi_f(\mathbf{k}_1, \mathbf{r}_1, \mathbf{k}_2, \mathbf{r}_2)|\phi_f(\mathbf{k}_1', \mathbf{r}_1, \mathbf{k}_2', \mathbf{r}_2)\rangle = \delta(\mathbf{k}_1 - \mathbf{k}_1')\delta(\mathbf{k}_2 - \mathbf{k}_2'). \quad (11)$$

In equation (8), the one electron two-centre continuum (TCC) wave function [29] is given by

$$T(\mathbf{k}_i, \mathbf{r}_j) = \exp(-\pi\alpha_i)(\Gamma(1 - \imath\alpha_i))^2 \frac{\exp(\imath\mathbf{k}_i\mathbf{r}_j)}{(2\pi)^{3/2}} \times {}_1F_1(\imath\alpha_i, 1, -\imath(k_i r_{ja} + \mathbf{k}_i\mathbf{r}_{ja})) \times {}_1F_1(\imath\alpha_i, 1, -\imath(k_i r_{jb} + \mathbf{k}_i\mathbf{r}_{jb})). \quad (12)$$

It describes a slow electron in the field of two Coulomb centres. Here

$$\alpha_i = -\frac{Z_i}{k_i}, \quad \mathbf{r}_{ja} = \mathbf{r}_j + \boldsymbol{\rho}/2, \quad \mathbf{r}_{jb} = \mathbf{r}_j - \boldsymbol{\rho}/2, \quad i, j = 1, 2, \quad (13)$$

and $Z_i = 1$. Finally $\varphi_i(\mathbf{r}_1, \mathbf{r}_2)$ represents the space part of the initial state wave function.

Taking into account the symmetry of the final and initial functions with respect to exchange of $\mathbf{r}_1$ and $\mathbf{r}_2$, we can reduce the expression of the transition matrix element to the following six dimensional integral

$$T_{fi} = \sqrt{2}\int \mathbf{dr}_1 \int \mathbf{dr}_2 \bar{\phi}_f(\mathbf{r}_1, \mathbf{r}_2) V \varphi_i(\mathbf{r}_1, \mathbf{r}_2). \quad (14)$$

The space coordinates of the wave functions are defined in the molecular frame of reference, whose origin is fixed on the centre of mass of the molecule and whose z-axis is parallel to the internuclear vector $\boldsymbol{\rho}$ of constant modulus.

3. The initial state wave functions

3.1. The case of H_2

To show the importance of the initial state correlation, we consider three different variational wave functions for the

initial $^1\Sigma_g$ fundamental electronic state of H_2. We first apply the most elementary Heitler–London [37] wave function

$$\varphi_i(\mathbf{r}_1,\mathbf{r}_2) = N(\rho)[a_1 b_2 + a_2 b_1],$$
$$a_i = \sqrt{\frac{\lambda^3}{\pi}}\,\mathrm{e}^{-\lambda r_{ia}}, \quad b_i = \sqrt{\frac{\lambda^3}{\pi}}\,\mathrm{e}^{-\lambda r_{ib}}, \tag{15}$$
$$N(\rho) = \frac{1}{\sqrt{2(1+S^2)}}, \quad S = \frac{\mathrm{e}^{-\lambda\rho}}{3}[\rho^2\lambda^2 + 3\rho\lambda + 3], \quad \lambda = 1.$$

Here the ground state energy $E_i = -1.115$ au at the internuclear equilibrium distance $\rho = 1.56$ au. The comparison of the results obtained by this function with those given in [20] will permit us to verify our procedure.

We then apply the Mueller–Eyring wave function borrowed from [38]

$$\varphi_i(\mathbf{r}_1,\mathbf{r}_2) = N(\rho)[\phi(1)\psi(2) + \psi(1)\phi(2)]$$
$$\phi(j) = x_a(j) + \epsilon x_b(j), \quad \psi(j) = \epsilon x_a(j) + x_b(j),$$
$$x_a(j) = \exp(-\beta\xi_j - \gamma\eta_j), \quad x_b(j) = \exp(-\beta\xi_j + \gamma\eta_j),$$
$$\xi_j = \frac{r_{ja} + r_{jb}}{\rho}, \quad \eta_j = \frac{r_{ja} - r_{jb}}{\rho},$$
$$\beta = 0.835,\ \gamma = 0.775,\ \epsilon = 0.137,\ N(\rho) = 0.255 \tag{16}$$

for which the ground state energy $E_i = -1.149$ au at the internuclear distance $\rho = 1.4$ au.

The Turbiner–Guevara wave function [39], gives the best energy value $E_i = -1.174\,4196$ au for the internuclear distance $\rho = 1.4$ au. It is obtained by a variational method having 14 parameters and includes the electron–electron separation r_{12}

$$\Psi(\vec{r}_1,\vec{r}_2) = A_1\psi_1 + A_2\psi_2 + A_3\psi_3,$$
$$\psi_1 = (1+\hat{P}_{12})(1+\hat{P}_{ab}) \times \exp(-\alpha_1 r_{1a} - \alpha_2 r_{1b} - \alpha_3 r_{2a} - \alpha_4 r_{2b} - \gamma_1 r_{12}),$$
$$\psi_2 = (1+\hat{P}_{12}) \times \exp(-\alpha_5 r_{1a} - \alpha_6 r_{1b} - \alpha_6 r_{2a} - \alpha_5 r_{2b} - \gamma_2 r_{12}),$$
$$\psi_3 = (1+\hat{P}_{12}) \times \exp(-\alpha_7 r_{1a} - \alpha_7 r_{1b} - \alpha_8 r_{2a} - \alpha_8 r_{2b} - \gamma_3 r_{12}). \tag{17}$$

Here $\hat{P}_{12}$ and $\hat{P}_{ab}$ are the operators that interchange electrons ($1 \leftrightarrow 2$) and the two nuclei ($a \leftrightarrow b$), respectively. As we will see later in the results, this function will modify the behaviour of the MDCS obtained by the Heitler–London wave function presented in [20], that we reproduced also. This shows the necessity of introducing the initial state electron–electron correlation in the transition matrix element.

3.2. The case of N_2

The initial ground state configuration of N_2 is given by [40]

$$1\sigma_g^2 1\sigma_u^2 2\sigma_g^2 2\sigma_u^2 3\sigma_g^2 1\pi_u^4. \tag{18}$$

The molecular orbitals σ_g, σ_u and π_u-type mentioned above are constructed by linear combinations of the following double Slater type 1s, 1s′, 2s, 2s′, 2p, 2p′ and single Slater type 3d atomic orbitals [40] for the internuclear distance $\rho = 2.0675$ au:

$$1s = \sqrt{\frac{\xi_1^3}{\pi}}\exp(-\xi_1 r), \quad 1s' = \sqrt{\frac{\xi_2^3}{\pi}}\exp(-\xi_2 r),$$
$$2s = \sqrt{\frac{\xi_3^5}{3\pi}}\,r\exp(-\xi_3 r), \quad 2s' = \sqrt{\frac{\xi_4^5}{3\pi}}\,r\exp(-\xi_4 r),$$
$$2p_z = \sqrt{\frac{\xi_5^5}{\pi}}\,z\exp(-\xi_5 r), \quad 2p'_z = \sqrt{\frac{\xi_6^5}{\pi}}\,z\exp(-\xi_6 r),$$
$$3d_{zz} = \sqrt{\frac{\xi_7^7}{18\pi}}\,(2z^2 - x^2 - y^2)\exp(-\xi_7 r),$$
$$2p_x = \sqrt{\frac{\xi_8^5}{\pi}}\,x\exp(-\xi_8 r), \quad 2p'_x = \sqrt{\frac{\xi_9^5}{\pi}}\,x\exp(-\xi_9 r),$$
$$2p_y = \sqrt{\frac{\xi_8^5}{\pi}}\,y\exp(-\xi_8 r), \quad 2p'_y = \sqrt{\frac{\xi_9^5}{\pi}}\,y\exp(-\xi_9 r),$$
$$3d_{xz} = \sqrt{\frac{2\xi_{10}^7}{3\pi}}\,x\,z\exp(-\xi_{10} r),$$
$$3d_{yz} = \sqrt{\frac{2\xi_{10}^7}{3\pi}}\,y\,z\exp(-\xi_{10} r). \tag{19}$$

The σ_g, σ_u and π_u-type molecular orbitals are given respectively by

$$\psi_i^g = c_{i1}\frac{1s_a + 1s_b}{\sqrt{2}} + c_{i2}\frac{1s'_a + 1s'_b}{\sqrt{2}} + c_{i3}\frac{2s_a + 2s_b}{\sqrt{2}} + c_{i4}\frac{2s'_a + 2s'_b}{\sqrt{2}} + c_{i5}\frac{2p_{z_a} - 2p_{z_b}}{\sqrt{2}} + c_{i6}\frac{2p'_{z_a} - 2p'_{z_b}}{\sqrt{2}} + c_{i7}\frac{3d_{zz_a} + 3d_{zz_b}}{\sqrt{2}}, \quad i = 1,3,5,$$
$$\psi_i^u = c_{i1}\frac{1s_a - 1s_b}{\sqrt{2}} + c_{i2}\frac{1s'_a - 1s'_b}{\sqrt{2}} + c_{i3}\frac{2s_a - 2s_b}{\sqrt{2}} + c_{i4}\frac{2s'_a - 2s'_b}{\sqrt{2}} + c_{i5}\frac{2p_{z_a} + 2p_{z_b}}{\sqrt{2}} + c_{i6}\frac{2p'_{z_a} + 2p'_{z_b}}{\sqrt{2}} + c_{i7}\frac{3d_{zz_a} - 3d_{zz_b}}{\sqrt{2}}, \quad i = 2,4,$$
$$\phi_i^x = c_{i8}\frac{2p_{x_a} + 2p_{x_b}}{\sqrt{2}} + c_{i9}\frac{2p'_{x_a} + 2p'_{x_b}}{\sqrt{2}} + c_{i10}\frac{3d_{xz_a} - 3d_{xz_b}}{\sqrt{2}}, \quad i = 6,$$
$$\phi_i^y = c_{i8}\frac{2p_{y_a} + 2p_{y_b}}{\sqrt{2}} + c_{i9}\frac{2p'_{y_a} + 2p'_{y_b}}{\sqrt{2}} + c_{i10}\frac{3d_{yz_a} - 3d_{yz_b}}{\sqrt{2}}, \quad i = 6. \tag{20}$$

The optimized orbital exponents ξ_j, $j = 1-10$ [40], and the corresponding coefficients of the molecular orbitals, which have been obtained by the Fortran code STOP [41, 42], are shown in table 1. Our calculations are performed with relative accuracy 10^{-5}. The comparison of the calculated orbital energies, and the total energy values with those given in [40, 43, 44] are displayed in table 2.

The initial wave function describing the valence electrons of the $3\sigma_g$ orbital is given by

$$\varphi_i(\mathbf{r}_1,\mathbf{r}_2) = 3\sigma_g(\mathbf{r}_1)3\sigma_g(\mathbf{r}_2) \equiv \psi_5^g(\mathbf{r}_1)\psi_5^g(\mathbf{r}_2). \tag{21}$$

In contrast to the case of diatomic hydrogen for which many highly correlated wave functions are available, we will, at

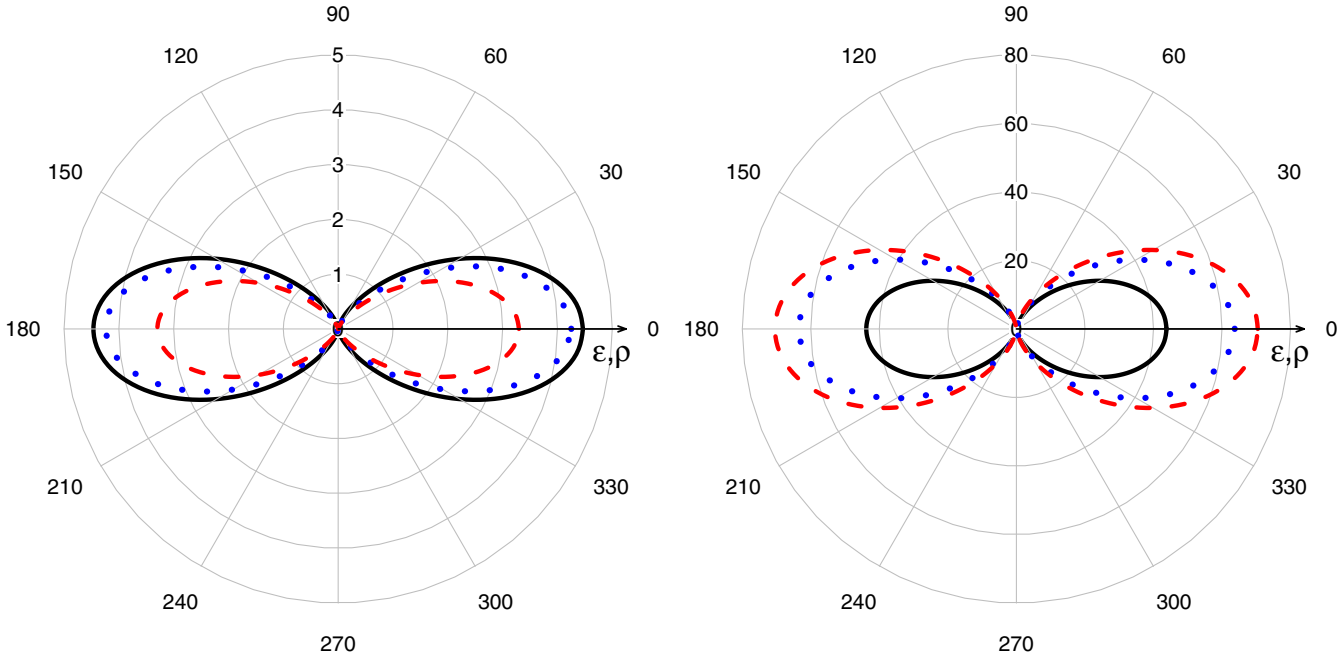

Figure 1. The variation, in polar representation, of the fourfold differential cross section in atomic units equation (1), scaled by 10^5, of the photo-double ionization of H_2 obtained by the velocity gauge (left) and the length gauge (right). The polar angle represents the ejection angle θ_2. Here $E_1 = E_2 = 10$ eV and the polarization vector $\boldsymbol{\epsilon}$ is parallel to the internuclear axis $\boldsymbol{\rho}$; $\mathbf{k}_2$, $\boldsymbol{\epsilon}$, $\boldsymbol{\rho}$ are coplanar and $\mathbf{k}_1$ is perpendicular to them. (cf [20] figure 8(a).) The solid line gives the results obtained by the Turbiner–Guevara wave function, the dotted line those obtained by the Mueller–Eyring wave function and the dashed line those obtained by the Heitler–London wave function.

Table 1. The basis exponents and coefficients for N_2.

			$1\sigma_g$	$1\sigma_u$	$2\sigma_g$	$2\sigma_u$	$3\sigma_g$	$1\pi_u$
ξ_1	6.212 92	c_{i1}	0.858 87	0.859 12	−0.302 67	−0.254 63	0.071 39	
ξ_2	9.368 27	c_{i2}	0.147 54	0.147 73	0.026 56	0.018 70	0.000 63	
ξ_3	1.467 86	c_{i3}	−0.000 37	−0.006 05	0.083 23	0.430 95	−0.399 26	
ξ_4	2.246 42	c_{i4}	0.003 23	0.003 65	0.604 23	0.657 87	−0.236 94	
ξ_5	1.528 53	c_{i5}	−0.000 17	−0.004 03	0.239 54	−0.275 66	0.637 48	
ξ_6	3.336 78	c_{i6}	0.002 41	0.002 68	0.158 70	−0.139 60	0.287 82	
ξ_7	1.935 00	c_{i7}	0.000 84	−0.000 20	0.095 60	0.005 93	0.083 90	
ξ_8	1.528 53	c_{i8}						0.650 87
ξ_9	3.336 78	c_{i9}						0.251 09
ξ_{10}	2.437 00	c_{i10}						0.073 59

Table 2. The molecular orbital energies and total energy of N_2.

	Present	[40]	[43]	[44]
$1\sigma_g$	−15.695 86	−15.696 23	−15.681 95	−15.721 88
$1\sigma_u$	−15.692 25	−15.692 62	−15.678 33	−15.719 78
$2\sigma_g$	−1.486 70	−1.485 69	−1.473 60	−1.452 70
$2\sigma_u$	−0.787 60	−0.785 81	−0.779 60	−0.730 59
$3\sigma_g$	−0.647 73	−0.642 78	−0.642 78	−0.544 58
$1\pi_u$	−0.621 38	−0.622 61	−0.615 54	−0.579 73
Total energy	−108.978 54	−108.971 43	−108.992 80	−108.823 00

this stage, apply only the above diatomic Hartree–Fock wave function for the case of diatomic nitrogen in the frozen core model. Applying models of wave functions going beyond Hartree–Fock and including the electron–electron separation r_{12} is somewhat more complicated and time consuming but not impossible. We will undertake this task in future calculations.

4. Results

In what follows we take the propagation of the linearly polarized photon in the x direction with the polarization vector $\boldsymbol{\epsilon}$ parallel to the z axis of the laboratory frame. The orientation of the internuclear axis, which will be considered as fixed during the ionization process, will be given by the polar θ_ρ and azimuthal φ_ρ angles with respect to the laboratory frame.

We begin by verifying our procedure first by reproducing exactly the results concerning the $(\gamma, 2e)$ photo-double ionization of H_2 given by [20], which are obtained by applying the velocity gauge and using the simple Heitler–London wave function. These are given by the curves with dashed lines in figures 1–4.

In figure 1, concerning the situation $\boldsymbol{\epsilon} \uparrow\uparrow \boldsymbol{\rho}$, we also present the results obtained by the length gauge. We observe that in this case the length gauge produces the same structure as the velocity gauge with a magnitude about ten times bigger for the result obtained by the Turbiner–Guevara wave function,

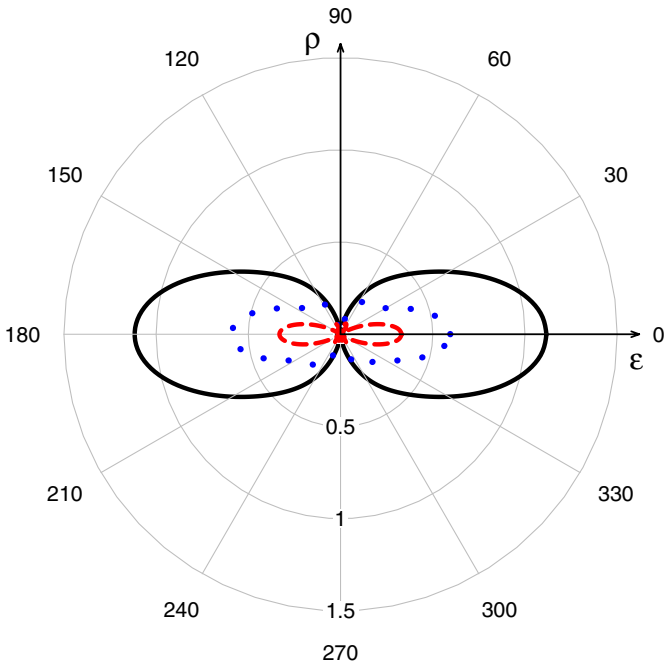

Figure 2. Same as in figure 1, for $\boldsymbol{\rho} \perp \boldsymbol{\epsilon}$. The results are obtained by the velocity gauge. Here the cross section with the Heitler–London wave function is multiplied by 1.5. (cf [20] figure 8(d).)

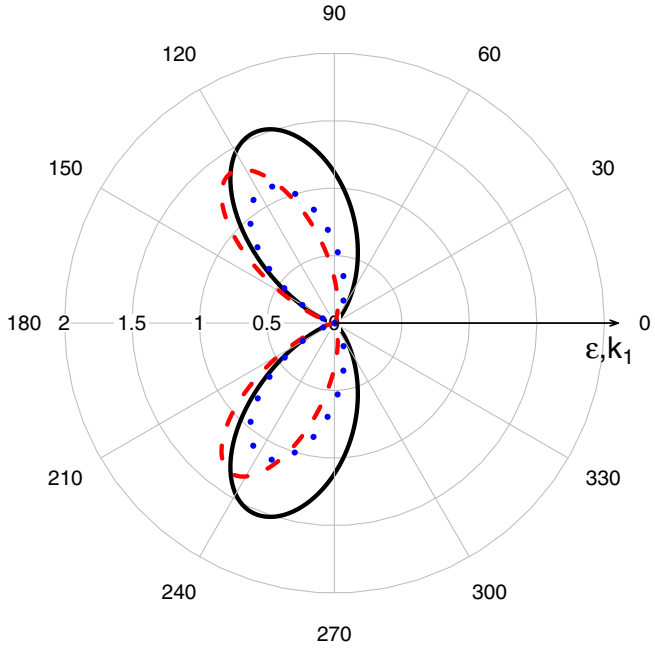

Figure 3. Same as in figure 1, for $\boldsymbol{\epsilon} \uparrow\uparrow \mathbf{k}_1$; $\mathbf{k}_2$ coplanar with $\boldsymbol{\epsilon}$, $\mathbf{k}_1$ and $\boldsymbol{\rho}$ is perpendicular to them. (cf [20] figure 10(a).) The results are obtained by the velocity gauge.

about 15 times for those obtained by the Mueller–Eyring wave function and about 20 times for those obtained by the Heitler–London wave function. This shows that the quality of the initial state function plays an important role, and that it is not the only factor. It is now admitted that the coincidence of the results obtained by the length and velocity gauges for low ejection energy values is an excellent check for the quality of the initial and also of the final state wave function. As an example one can see the good agreement between the

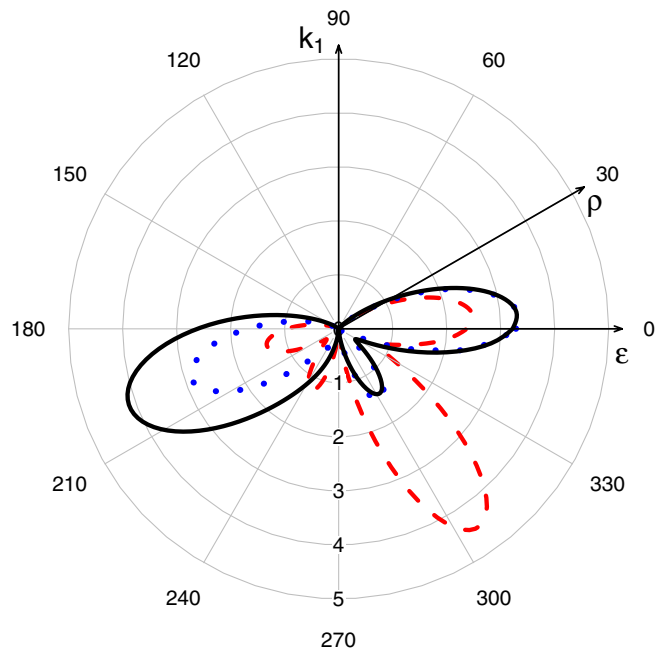

Figure 4. Same as in figure 1, for $\mathbf{k}_1 \perp \boldsymbol{\epsilon}$; $\boldsymbol{\rho}$ is coplanar with $\boldsymbol{\epsilon}$. (cf [20] figure 11(b).) The results are obtained by the velocity gauge.

results concerning the oscillator strength of He obtained by three different gauges given in [45]. Other examples of such coincidences can be found also in numerical convergent close coupling calculations [46] or time-dependent close coupling [47]. The examples, for which the two gauges do not produce similar results, are numerous. We can mention the results of Byron and Joachian in [48], Le Rouzo [49], Kornberg and Miraglia [50] in the case of helium, and those of Kheifets in the case of Be [16]. Now the reason of this disagreement between the results of the different gauges can be diverse. The quality of the wave functions should play the most important role. There is also the fact that the velocity gauge is supposed to be more appropriate to the cases of higher energy values [51]. Kheifets and Bray in [16] explain the disagreement between the results of the length and velocity gauges by the fact that they have used the frozen core model for Be. Now coming back to our case of H_2, where the description of the double continuum in the final state is much more difficult, we think that the disagreement could be due to the final state wave function, which is given in the form of a correlated product of the TCC wave function, which satisfies the correct asymptotic conditions, but does not represent an exact solution of the problem. The disagreement can also result from the fact that the length gauge is less appropriate for the considered energy domain as we mentioned above [51].

In figure 2 the structure of the curves obtained by the three wave functions remains quite similar also, but the curve obtained by the Heitler–London wave function presents four lobes—two of them very small—which are attenuated in the case of Mueller–Eyring and disappear completely in the Turbiner–Guevara case.

In figure 3 the differences between the results of the three initial state wave functions become somewhat more visible. The three lobes do not have the same optimal directions for

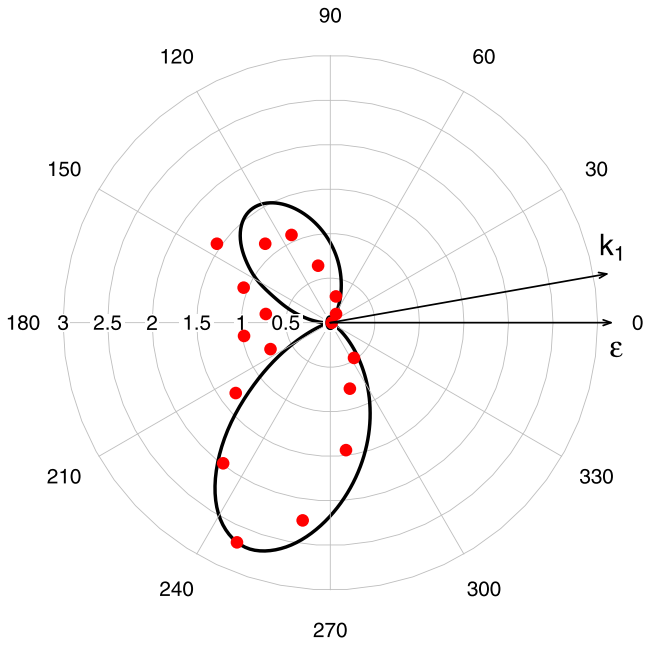

Figure 5. The variation, in polar representation, of the FDCS in atomic units equation (2), scaled by 10^5, of the photo-double ionization of H_2 in the velocity gauge obtained by the Turbiner–Guevara wave function. The polar angle represents the θ_2 of the ejected electron. Here $E_1 = E_2 = 12.5$ eV and $\theta_1 = 10^\circ$. The experimental data are from Weber [52]. (cf [21] figure 4.)

$\mathbf{k}_2$. In figure 4 the disagreement is more pronounced. This verifies once more the fact that the initial state electron–electron correlation is an important factor in this process. This was pointed out in the very early stages of photo-double ionization in [1].

In figure 5 we present the variation of the TDCS for randomly oriented targets in atomic units obtained by the velocity gauge for $E_1 = E_2 = 12.5$ eV compared to the experimental results of Weber [52] extracted from [21]. Here we have used the Turbiner–Guevara wave function, which we admit is the most reliable, as it includes the electronic correlation best. The polarization vector and the wave vectors of the ejected electrons lie in the plane of the figure. The ejection angle of one of the photoelectrons is fixed at $\theta_1 = 10^\circ$ with respect to the polarization vector, and the second angle θ_2 is chosen as the polar angle of the curve. Here, all molecular orientations are taken into account. The experimental results are scaled in such a way to have the theoretical and experimental maxima around 250° of the same size.

Once we have tested our procedure and observed that it produces the experimental results quite well, we pass to the photo-double ionization of N_2 in the equal ejection energy regime. Here we will also consider the photo-double ionization of N_2 as a vertical transition from the fundamental electronic state of the neutral target at its equilibrium internuclear distance to the fundamental $^1\Sigma_g$ state of the residual N_2^{2+} dication. The case of the photo-double ionization to the neighbouring $^3\Pi_u$ final state of N_2^{2+}—which should contribute to the results in experiments—have low energy resolution and cannot distinguish between the two possible events (see [31, 32]). The present work is a first tentative one to tackle the photo-double ionization of N_2 by the correlated TCC function. We will apply, at this stage, the wave function described in section 3.2, which is constructed by the Hartree–Fock diatomic orbital (see equation (21)). Higher quality wave functions including the electron–electron separation r_{12} are more difficult to obtain, and their application is much more time consuming. We will undertake this work in a future paper. Our results will be compared to those obtained by the best fit of the following Gaussian parametrization

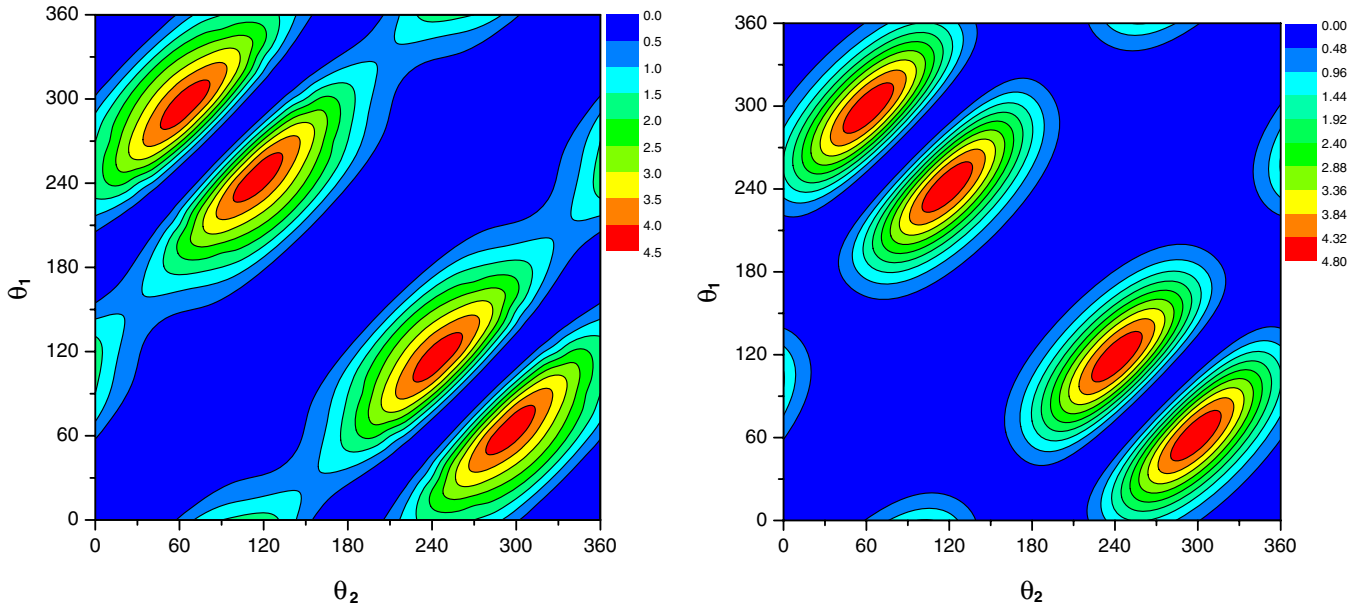

Figure 6. Left: greyscale representation (colourscale in the online version) of the variation of the TDCS in atomic units equation (2), scaled by 10^4, of the photo-double ionization of the $3\sigma_g$ level of N_2 obtained by the velocity gauge in terms of the two ejection angles θ_1 and θ_2. Here $E_1 = E_2 = 10$ eV, and the vectors $\mathbf{k}_1$, $\mathbf{k}_2$, $\boldsymbol{\epsilon}$ lie in the same plane. Right: the equivalent representation obtained by the Gaussian parametrization fit.

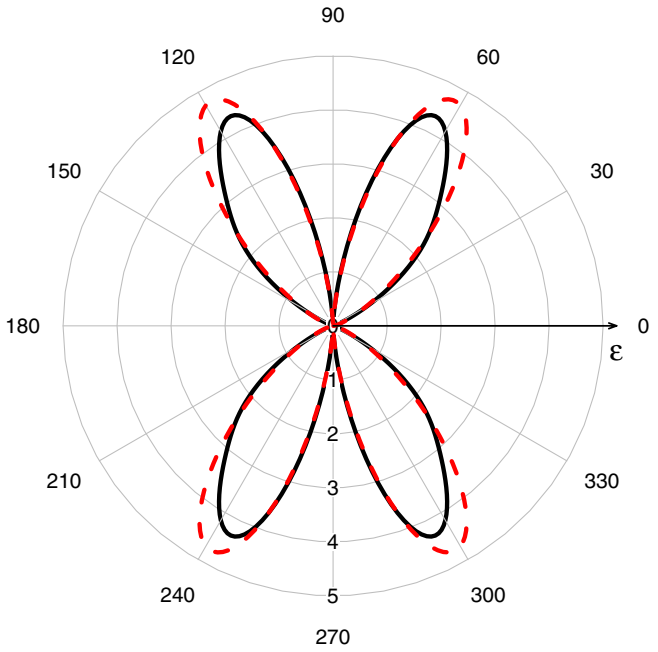

Figure 7. Polar representation of the variation of the TDCS in atomic units, scaled by 10^4, of the photo-double ionization of the $3\sigma_g$ orbital of N_2 obtained by the velocity gauge. The polar angle represents the θ_2 of the ejected electron. Here $\theta_1 = 2\pi - \theta_2$, $E_1 = E_2 = 10$ eV, and the vectors $\mathbf{k}_1$, $\mathbf{k}_2$, $\boldsymbol{\epsilon}$ lie in the same plane. The solid line represents the results obtained by equation (2). The dashed line shows those obtained by the Gaussian parameterization.

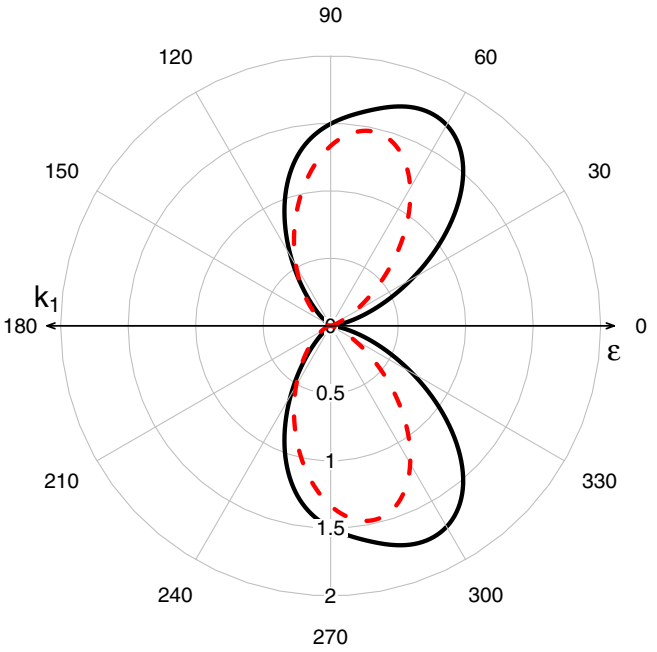

Figure 8. Same as in figure 7 but with a fixed value of $\theta_1 = 180^\circ$.

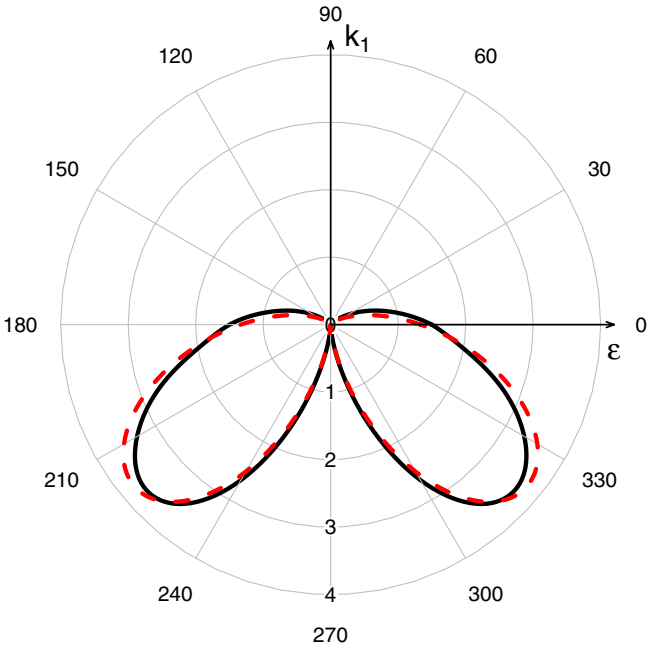

Figure 9. Same as in figure 7 but with a fixed value of $\theta_1 = 90^\circ$.

formula [53]

$$f(\theta_1,\theta_2) = a\,(\cos(\theta_1)+\cos(\theta_2))^2 \times \exp\left[-4\ln(2)\frac{(\theta_{12}-180^\circ)^2}{\Gamma^2}\right], \quad \theta_{12} = |\theta_1-\theta_2|. \quad (22)$$

The fitting is done by minimizing the following function with respect to the parameters a, Γ, using a comprehensive modified Newton algorithm:

$$F(a,\Gamma) = \frac{1}{37^2}\sum_{i,j=1}^{37}\left(\sigma^{(3)}(\theta_1^i,\theta_2^j) - f(\theta_1^i,\theta_2^j)\right)^2 \longrightarrow_{a,\Gamma} \min,$$

$$\theta_1^i = 10^\circ(i-1), \quad \theta_2^j = 10^\circ(j-1), \quad (23)$$

with $\sigma^{(3)}(\theta_1^i,\theta_2^j)$ representing our calculated TDCS. The reached accuracy is 10^{-6}. This gives the best correlation factor width $\Gamma = \Gamma(E) = 1.7346 = 99.4^\circ$ and

$$a = a(E) = 1.2945\times10^{-3}, \quad F(a,\Gamma) = 1.0029\times10^{-1}. \quad (24)$$

Figure 6 gives, in the greyscale representation (colourscale in the online version), the variation of the TDCS for the photo-double ionization of the $3\sigma_g$ orbital of N_2 in terms of the two ejection angles for $E_1 = E_2 = 10$ eV. Here the vectors $\mathbf{k}_1$, $\mathbf{k}_2$ and $\boldsymbol{\epsilon}$ lie in the same plane. On the left we present our results, and on the right those obtained by the parameterization formula. We observe that, on the two curves, the symmetry $\sigma^{(3)}(\theta_1,\theta_2) = \sigma^{(3)}(\theta_2,\theta_1)$ is respected. Then the diagonal $\theta_1 = \theta_2$ is an axis of symmetry, as we obtain practically the same structure on both sides of this line. We must mention here that perfect symmetry on the figure corresponding to our results is obtained by employing accurate integration over the molecular orientations. We also observe that the second diagonal line defined by $\theta_1 + \theta_2 = 2\pi$ is also a symmetry axis as expected. In the same manner, the lines $\theta_1 = \theta_2 \pm \pi$ have the same structure on both of their sides as expected also.

These symmetry situations can also be observed on the three polar representations of figures 7–9, where we have plotted the results of the two types of calculations to show their differences. In figure 7, where $\theta_1 + \theta_2 = 2\pi$ and $E_1 = E_2$, the four lobes of each curve are identical, as expected. In contrast to the atomic case of He, we observe here the deflection of the calculated TDCS from the Gaussian distribution.

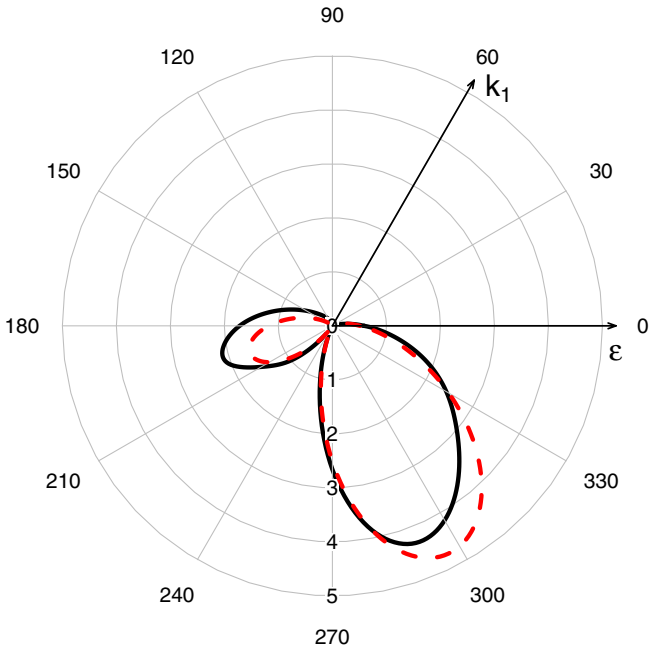

Figure 10. Same as in figure 7 but with a fixed value of $\theta_1 = 60^\circ$.

Figures 8 and 9 present two particular situations in polar representation at respectively $\theta_1 = 180^\circ$ and $\theta_1 = 90^\circ$. Here the deflection of our results from the Gaussian shape is also evident. In the first case, the electron with wave vector $\mathbf{k}_1$, is ejected in the direction of $\boldsymbol{\epsilon}$ and in the second, perpendicular to it. We see that, as expected, the latter geometry, which puts $\mathbf{k}_1$ far from the polarization vector $\boldsymbol{\epsilon}$, is more efficient. Finally, in figure 10, we show the variation for the situation, which gives the largest lobe with respect to the preceding cases. This happens for $\theta_1 = 60^\circ$. Here the comparison with the results of the Gaussian parametrization also shows a deflection, which is very similar to the one observed for the experimental results concerning the photo-double ionization of D_2 for the same ejection energy values of (see figure 3 in [18]).

5. Conclusion

We have determined the fourfold and triple differential cross sections, corresponding respectively to the oriented and randomly oriented diatomic molecules, of the photo-double ionization of H_2 and N_2 diatomic systems, in the equal ejection energy regime, by applying the correlated product of two TCC functions, to describe the two equivalent ejected electrons, which has the advantage of showing the influence of the final state electron–electron correlation. We have applied three different initial state wave functions for the fundamental state of H_2, shown the importance of the initial state correlation and obtained quite good agreement with the experimental results. In the case of N_2, basic Hartree–Fock diatomic orbitals are obtained and applied as a first attempt. The results verify the symmetry conditions of the TDCS and show the optimal ejection directions for an equal energy sharing geometry. The comparison with the fitted Gaussian parametrization results show some instructive deflections due to the diatomic nature of the targets. The case of unequal ejection energy, and the neighbouring $^3\Pi_u$ state of N_2^{2+}, which presents open shell configurations will be treated in a near future paper.

Acknowledgments

The authors are grateful to A G Galstyan for useful discussions and help. This work was partially supported by the RFBR grant no 11-01-00523, and the theme 09-6-1060-2005/2013 'Mathematical support of experimental and theoretical studies conducted by JINR'.

References

[1] Byron F W Jr and Jochain C J 1966 *Phys. Rev. Lett.* **16** 1139–42
[2] McGuire H 1997 *Electron Correlation and Dynamics in Atomic Collisions* (Cambridge: Cambridge University Press)
[3] Schmidt V 1998 *Pramana J. Phys.* **50** 501–14
[4] Schwarzkopf O, Krässig B, Eimiger J and Schmidt V 1993 *Phys. Rev. Lett.* **70** 3008–11
[5] Dawber G, Avaldi L, McConkey A G, Rojas H, MacDonald M A and King G C 1995 *J. Phys. B: At. Mol. Opt. Phys.* **28** L271–8
[6] Dörne R *et al* 1998 *Phys. Rev.* A **57** 1074–90
[7] Bolognesi P, Zitnik M, Malegat L, Selles P, Turri G, Coreno M, Camilloni R and Avaldi L 2004 *J. Phys. B: At. Mol. Opt. Phys.* **37** 2285–302
[8] Knapp A *et al* 2005 *J. Phys. B: At. Mol. Opt. Phys.* **38** 615–33
[9] Penent F, Lablanquie P, Palaudoux J, Gamblin G, Andric L, Ito K, Hikosaka Y, Kaneyasu T and Eland J H D 2009 *Eur. Phys. J. Spec. Top.* **169** 73–78
[10] Otranto S and Garibotti C R 2002 *Eur. Phys. J.* D **21** 285–91
[11] Briggs J S and Schmidt V 2000 *J. Phys. B: At. Mol. Opt. Phys.* **33** R1–R48
[12] Maulbetsch F and Briggs J S 1994 *J. Phys. B: At. Mol. Opt. Phys.* **27** 4095–104
[13] Kornberg M A and Rodriguez V D 1999 *Eur. Phys. J.* D **5** 221–4
[14] Chandra N and Sen S 1999 *Eur. Phys. J.* D **6** 457–80
[15] Malegat L, Selles P and Kazansky A 2000 *Phys. Rev. Lett.* **85** 4450–3
[16] Kheifets A S and Bray I 2007 *Phys. Rev.* A **75** 042703
[17] Das J N, Paul S and Chakrabati K 2006 *Eur. Phys. J.* D **39** 223–5
[18] Wightman J P, Cvejanovic S and Reddish T J 1999 *J. Phys. B: At. Mol. Opt. Phys.* **31** 1753–64
[19] Iijima T, Bonham R A and Ando T 1963 *J. Phys. Chem.* **67** 1472–4
[20] Walter M and Briggs J 1999 *J. Phys. B: At. Mol. Opt. Phys.* **32** 2487–501
[21] Kheifets A S 2005 *Phys. Rev.* A **71** 022704
[22] Dörner R *et al* 1998 *Phys. Rev. Lett.* **81** 5776–9
[23] Ivanov I A and Kheifets A S 2011 *Phys. Rev.* A **83** 063411
[24] Ivanov I A and Kheifets A S 2012 *Phys. Rev.* A **85** 013406
[25] Masuoka T 1986 *Z. Phys.* D **4** 43–56
[26] Franceschi F, Ascenzi D, Tosi P, Thissen R, Žabka J, Roithová J, Ricketts C L, Simone M D and Coreno M 2007 *J. Chem. Phys.* **126** 134310
[27] Schöffler M S *et al* 2008 *Phys. Rev.* A **78** 013414
[28] Vanroose W, Horner D A, Martín F, Rescigno T N and McCurdy C W 2006 *Phys. Rev.* A **74** 052702
[29] Chuluunbaatar O, Joulakian B B, Puzynin I V, Tsookhuu Kh and Vinitsky S I 2008 *J. Phys. B: At. Mol. Opt. Phys.* **41** 015204
[30] Bellm S, Lower J, Weigold E and Mueller D W 2010 *Phys. Rev. Lett.* **104** 023202

[31] Eland J H D 2003 *Chem. Phys.* **294** 171–86
[32] Lundqvisty M, Edvardssonz D, Baltzery P and Wannbergy B 1996 *J. Phys. B: At. Mol. Opt. Phys.* **29** 1489–500
[33] Chuluunbaatar O, Gusev A A and Joulakian B B 2012 *J. Phys. B: At. Mol. Opt. Phys.* **45** 015205
[34] Lahmam-Bennani A, Duguet A, Dal Cappello C, Nebdi H and Piraux B 2003 *Phys. Rev.* A **67** 010701
[35] Chang E S and Fano U 1972 *Phys. Rev.* A **6** 173–85
[36] Joulakian B, Dal Cappello C and Brauner M 1992 *J. Phys. B: At. Mol. Opt. Phys.* **25** 2863–72
[37] Heitler W and London F 1927 *Z. Phys.* **44** 455–72
[38] Mueller C R and Eyring H 1951 *J. Chem. Phys.* **19** 1495–7
[39] Turbiner A V and Guevara N L 2007 arXiv:physics/0606120v2 [physics.atom-ph]
[40] Nesbet R K 1964 *J. Chem. Phys.* **40** 3619–33
[41] Bouferguène A, Fares M and Hoggan P E 1996 *Int. J. Quantum Chem.* **57** 801–10
[42] Bouferguène A and Hoggan P E 1996 STOP: a Slater-type orbital package *QCPE Program Number* **667**
[43] Cade P E, Sales K D and Wahl A C 1966 *J. Chem. Phys.* **44** 1973–2003
[44] Scherr C W 1955 *J. Chem. Phys.* **23** 569–78
[45] Stewart A L and Webb T G 1963 *Proc. Phys. Soc.* **82** 532–6
[46] Kheifets A S and Bray I 1996 *Phys. Rev.* A **54** R995–7
[47] Colgan J, Pindzola M S and Robicheaux F 2001 *J. Phys. B: At. Mol. Opt. Phys.* **34** L457–66
[48] Byron F W and Joachain C J 1967 *Phys. Rev.* **164** 1–9
[49] Le Rouzo H and Dal Cappello C 1991 *Phys. Rev.* A **43** 318–29
[50] Kornberg M A and Miraglia J E 1993 *Phys. Rev.* A **48** 3714–9
[51] Dalgarno A and Sadeghpour H R 1992 *Phys. Rev.* A **46** R3591–93
[52] Weber T 2003 *PhD Thesis* Institut für Kernphysik, Universität Frankfurt
[53] Huetz A, Selles P, Waymel D and Mazeau J 1991 *J. Phys. B: At. Mol. Opt. Phys.* **24** 1917–33